View metadata, citation and similar papers at core.ac.uk

brought to you by CORE

provided by Repository@Nottingham

Manuscript Details

Manuscript number	MECMAT_2019_241_R2
Title	Determination of Creep Damage Properties from Small Punch Creep Tests Using an Inverse Approach
Article type	Research Paper

Abstract

Although the small punch creep test (SPCT) has been commonly accepted as an effective small specimen material characterisation technique (e.g. the European Code of Practice (CoP) for small punch test was produced in 2006 to provide a practical guideline for the experimental work and data interpretation of small punch test), the conversion from the experimental results obtained from the SPCT, i.e. displacement-time data, to the corresponding strain-time data obtained from conventional uniaxial creep tests has not been thoroughly understood due to the complex nature of the deformation and material failure mechanisms involved in the SPCT, e.g. contact mechanism, material nonlinearity, large deformation and initial plasticity damage. The current paper presents an inverse method to determine the creep properties directly from the SPCT experimental results, without converting them to the uniaxial creep test data. A finite element (FE) model taking account of the conventionally overlooked pre-straining effects has been employed for an inverse optimisation method for the first time. The inverse method has been proven to be capable of effectively predicting the creep behaviours of a P91 steel at 600ºC with a good agreement to the experimental results.

Keywords	small punch creep test; creep damage properties; pre-straining effect; inverse approach
Manuscript region of origin	Europe
Corresponding Author	Wu Wen
Corresponding Author's Institution	University of Nottingham
Order of Authors	Wu Wen, Xiaozhe Jin, Hao Liu, Wei Sun
Suggested reviewers	Yingzhi Li, qiang xu, Kaishu Guan, Robert Lancaster, Haofeng Chen

Submission Files Included in this PDF

File Name [File Type]

Replay to editor (2nd revision).docx [Response to Reviewers]

Highlights.docx [Highlights]

MECMAT_2019_241 (2nd revised).docx [Manuscript File]

Author Agreement.docx [Author Agreement]

To view all the submission files, including those not included in the PDF, click on the manuscript title on your EVISE Homepage, then click 'Download zip file'.

Research Data Related to this Submission

There are no linked research data sets for this submission. The following reason is given:
Data will be made available on request

Dear Editor,

We are very grateful for your consideration of accepting this manuscript. We have added another paragraph to the Discussion section (highlighted in yellow) to address the meaning and importance of this study.

Regards,

Wu Wen

Highlights

- An inverse approach has been developed for determining the creep damage constitutive properties from small punch creep tests.
- The method involves the application of an optimization scheme in conjunct with finite element modelling.
- The initial plasticity straining effect has been taken into account for the first time in the inverse method.
- A demonstration has been presented to apply the inverse approach to determine the creep damage properties of a P91 steel at 600°C.

Determination of Creep Damage Properties from Small Punch Creep Tests Considering Pre-Straining Effect Using an Inverse Approach

Wu Wen, Xiaozhe Jin, Hao Liu, Wei Sun

Faculty of Engineering, University of Nottingham, Nottingham, NG7 2RD, UK

Corresponding author: Wu Wen

Address: Room C03, ITRC Building, University Park, Nottingham, NG7 2RD UK

Telephone: +44 (0)7526973730

E-mail: wenwu.gm2011@gmail.com

Declarations of interest: none

Abstract

Although the small punch creep test (SPCT) has been commonly accepted as an effective small specimen material characterisation technique (e.g. the European Code of Practice (CoP) for small punch test was produced in 2006 to provide a practical guideline for the experimental work and data interpretation of small punch test), the conversion from the experimental results obtained from the SPCT, i.e. displacement-time data, to the corresponding strain-time data obtained from conventional uniaxial creep tests has not been thoroughly understood due to the complex nature of the deformation and material failure mechanisms involved in the SPCT, e.g. contact mechanism, material nonlinearity, large deformation and initial plasticity damage.

The current paper presents an inverse method to determine the creep properties directly from the SPCT experimental results, without converting them to the uniaxial creep test data. A finite element (FE) model taking account of the conventionally overlooked pre-straining effect has been employed for an inverse optimisation method for the first time. The inverse method has been proven to be capable of effectively predicting the creep behaviours of a P91 steel at 600°C with a good agreement to the experimental results.

Keywords: small punch creep test; creep damage properties; Pre-straining effect; inverse approach

Nomenclature

Symbol	Unit	Description
A, B, N, χ, q_2, α		Liu-Murakami creep damage constitutive properties
a_p	mm	Radius of the receiving hole
E	MPa	Elastic modulus
K_{sp}		Loading force-stress correction factor for SPCT
P	N	Loading force
Δ	mm	Displacement
ν		Poisson's ratio
R_s	mm	Punch head radius
t_f	h	Time to failure
t_0	mm	Specimen thickness
t	h	Time
σ, σ_{EQ}, σ_1, σ_D	MPa	Stress, equivalent stress, maximum principal stress, rupture stress
ε, ε^c		Strain, creep strain
ω		Creep damage state variable
ϕ , ψ		Pre-straining coefficients

1. Introduction

An elevated operating temperature is unavoidable or desired for many engineering applications, e.g. power plants, chemical plants, aero-engines and gas turbines. Creep strains and creep damage may occur and lead to structural failure when the components operate at high temperature for an extended period of time. It is crucial to assess the material degradation and estimate the remaining life to failure of the components subjected to creep damage. This information is usually captured by performing standard uniaxial creep tests. However, it requires to produce standard test specimens which are not always possible. In some cases, it is desired to characterise the local material behaviours without greatly compromising the structural integrity of the components in service, e.g. coatings, welds and the heat affected zone (HAZ) of a weld. In some other cases, the amount of a material available may be limited, e.g. a new material in the process of development. Therefore, various small specimen test and non-destructive testing (NDT) techniques have been widely employed for material characterisation and component life assessment [1, 2]. Small punch creep test (SPCT) is one of the most popular methods (e.g. [3-7]). The main advantage of SPCT compared to other small specimen creep testing techniques, such as small ring creep test and impression creep test, is that the full creep stages, including the primary, the secondary and the tertiary stage, are produced. To improve the understanding of SPCT as a material characterisation method, many researchers have carried out experimental (e.g. [3, 4, 6, 7]) and numerical studies (e.g. [6, 8-10]).

The most challenging part for SPCT technique is to correlate the results (i.e. the displacement-time data) to those of a conventional uniaxial creep test (i.e. the strain-time data) and hence obtain the creep constitutive parameters. This is because of the complexity of its deformation and failure mechanisms, i.e. contact mechanism, material nonlinearity, relatively high deformation and localised plasticity effects [11]. This interpretation issue of SPCT has been addressed in many studies (e.g. [11-14]). A code of practice (CoP) was developed to convert the load and displacement data from SPCT to the corresponding uniaxial stress and strain data in 2006 [14]. Although the empirical CoP has been used by researchers and industrial organizations, a universally accepted physically-based interpretation method for SPCT is still missing. Inverse approach has the potential to extract the creep properties from SPCT without converting the results to those of a uniaxial creep test. There are only a few studies on material characterisation by small punch test (SPT) using an inverse method, e.g. [15-20], in which the elastoplastic properties of the material are determined from the force-displacement data using a curve-fitting optimisation algorithm. Finite element (FE) analysis technique has been applied cooperatively with inverse methods in many cases [15-20]. A review on the essentials of the FE simulation techniques for SPT has been given by Abdendroth [21].

A notable phenomenon which occurs in the early stage of SPCT is the pre-straining, i.e. the localised plasticity. It should be noted that the effect of pre-straining on the creep behaviours has been neglected in most numerical simulations of SPCT while they have only been taken into consideration for FE modelling of SPCT by Cortellino et al [6] for the first time. It is suggested that the pre-existence of plasticity in the material has a significant influence on the subsequent creep deformation and the time to failure for a SPCT specimen, showing either creep resistance or creep enhancement and therefore cannot be neglected [6]. It is also shown that the accuracy of the predicted creep behaviour can be improved significantly by taking account of the pre-staining effect.

Inverse method is a powerful and interdisciplinary tool in a broad area of science and engineering study, including solid mechanics and fracture [22]. Finite element analysis has been an established assisting tool for inverse method application [23]. This approach has been employed to extract constitutive material properties from various of mechanical testing experiments, such as indentation tests [24], miniature specimen tensile tests [25] and small punch tensile tests [26]. The fundamental principle of this approach is to carry out iterative calculations based on the theoretical or empirical solutions or numerical simulations, such as finite element analysis, and to find the optimised material properties that give the best match to the

experimental results. One important motivation to apply inverse method is that in some cases the experimental results are not easily interpreted to derive direct relationships to the constitutive material properties, e.g. in the case of SPCT, it is hard to relate the time-displacement data directly to the creep damage properties due to the complex nature of possible early cracking, nonlinear contact behaviour, microstructural evolution and damage formation, etc, over the test. However, inverse method has not been commonly applied to SPCT interpretation (e.g. [27]). The feasibility of extracting creep properties from SPCT deformation data using an inverse method with FE analysis has been proved by Li et al [27]. It has been demonstrated that the inverse method with FE analysis delivers better predictions for the material properties than the commonly used method based on Chakrabarty' membrane theory. However, only the steady state creep, but not the creep damage evolution, has been considered in this model.

An effective inverse method to determine the complete creep properties with the considerations of the pre-straining effect is still needed. This paper presents an inverse approach to determine the complete creep properties from the creep deformation data of SPCT using an optimisation algorithm. A FE model of SPCT has been developed with the modified Liu-Murakami creep damage model [6, 28] taking account of the pre-straining effect. The SPCT FE model has been applied cooperatively with the inverse optimisation algorithm to determine the creep properties of a P91 steel from multiple sets of deformation data of SPCT carried out at 600°C.

2. Methodology

The objective of the current study is to develop an effective methodology to predict the creep behaviours and determine the creep properties from the SPCT. The investigation consists of a series of experiments (uniaxial tensile tests, uniaxial creep tests and SPCT), FE modelling and inverse optimisation work on the same material. Fig. 1 shows a flowchart of the current investigation. SPCT were carried out to provide the objective data set for the inverse algorithm. A 2D FE model was built for a standard SPCT. Uniaxial tensile and creep tests were carried out to obtain the reference material properties (for validation and initialization) for the FE modelling and the inverse optimisation. An inverse method was developed to take the data obtained from the experiments and FE modelling as the inputs and to predict the SPCT behaviour and to extract the creep properties of the material.

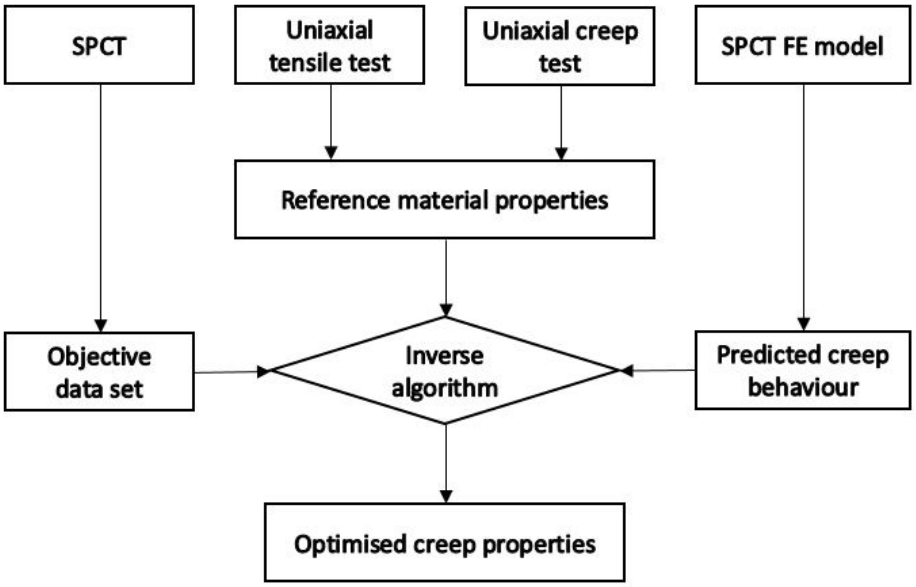

Fig. 1 Flowchart of the current investigation

2.1 Experiments

2.1.1 Material Chemical Composition and Microstructure

A series of experiments, including uniaxial tensile tests, uniaxial creep tests and SPCT, were carried out on a P91 steel at 600°C [6, 29]. The chemical composition of the P91 steel used in the experimental work is presented in Table 1 in wt% [25]. The material microstructure of the virgin P91 steel obtained from the clamped, undamaged region is shown by Fig. 2 [29]. The microstructure features homogeneous tempered martensite lathes with a number of finely distributed carbides, nitrides or carbo-nitrides along grain and sub-grain boundaries.

Table 1 Chemical composition (wt%) of the P91 steel used for the investigation [29]

Cr	Mo	C	Si	S	P	Al	V	Nb	N	W	Fe
8.60	1.02	0.12	0.34	<0.002	0.017	0.007	0.24	0.070	0.060	0.03	Bal

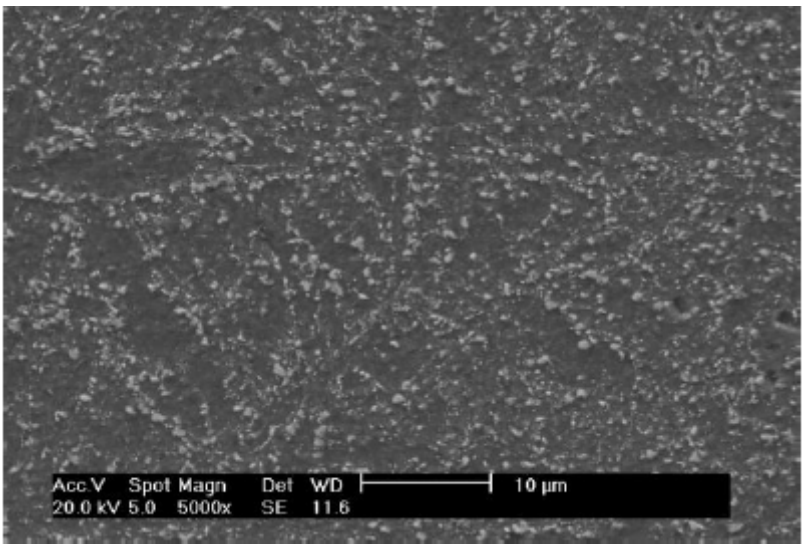

Fig. 2 SEM image of the original P91 steel [26].

2.1.2 Uniaxial Tensile and Creep Tests

The stress-strain curve obtained from the uniaxial tensile tests at 600°C on the P91 steel is shown by Fig. 3 [29]. These data provide the reference elastic-plastic properties of the P91 steel in the current investigation. Uniaxial creep tests were carried out at various stress levels from 140MPa to 180MPa. Fig. 4 shows the strain-time curves obtained from the uniaxial creep tests. Generally, the strain-time curves show the typical creep deformation/damage evolution: the primary stage with a decreasing strain rate, the secondary stage with the steady minimum strain rate and the tertiary stage with the increasing strain rate and the failure of the material. From the stress level of 140MPa to 180MPa, the minimum strain rate increases and the time to failure decreases.

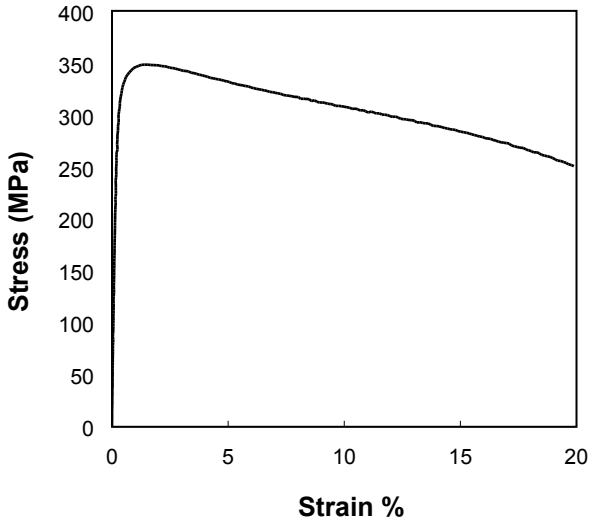

Fig. 3 True stress-strain curve for a P91 steel at 600°C [29].

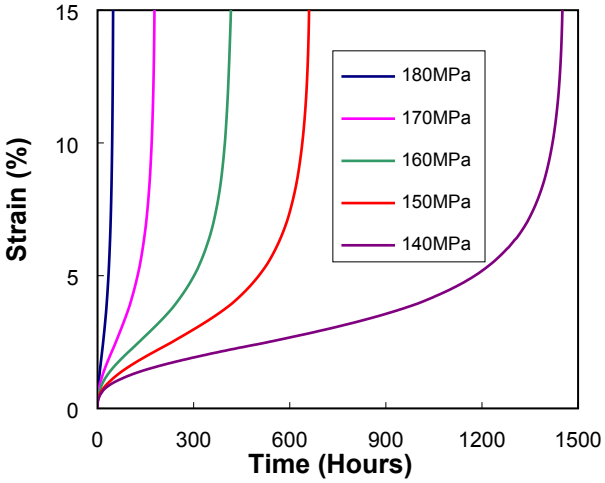

Fig. 4 Strain-time curves of the uniaxial creep tests at various stress levels for a P91 steel at 600°C [29].

2.1.3 Small Punch Creep Test

SPCT were carried out with the same P91 steel used for the uniaxial tensile/creep tests at five different load levels: 25kg, 28kg, 30kg, 34kg and 40kg [6]. A schematic illustration of SPCT is shown in Fig. 5, where the punch radius R_s=1.25mm, the lower clamp radius R_c=0.25mm, the receiving hole radius a_p=2mm, the original diameter D_0=8mm and the thickness of the disc specimen t_0=0.5mm.

The empirical relationships from the CoP [14] are shown by equations (1)-(3), where P is the applied load, Δ is the total deformation, σ is the membrane stress, ε is the strain at the edge of contact, R_s is the punch radius (R_s=1.25mm), t_o is the original specimen thickness (t_o=0.5mm), a_p is the distance between the punch centre and the clamps (a_p=2mm) and K_{sp} is a non-dimensional correction factor, determined empirically for the particular material.

$$\frac{P}{\sigma} = 1.72476\Delta - 0.05638\Delta^2 - 0.17688\Delta^3 \qquad (1)$$

$$\varepsilon = 0.7959\Delta + 0.09357\Delta^2 - 0.0044\Delta^3 \qquad (2)$$

$$\sigma = \frac{0.3P{a_p}^{0.2}}{K_{sp}{R_s}^{1.2}t_o} \quad (3)$$

With the above equations the uniaxial creep tests data can be used as a reference to estimate the required load level, i.e. the force to be applied to the punch, for the SPCT to be carried out on the same material for the same time to failure. Also, creep constitutive parameters can be extracted from the uniaxial strain-time curves with a suitable creep damage model, e.g. Liu-Murakami's model [28], to provide the reference creep parameters for FE modelling of the SPCT on the same material.

Fig. 6 shows the displacement-time curves obtained from the SPCT. The fluctuations in displacement found in the primary stage of creep at the load of 25kg, shown in Fig. 6, were due to the electronical noise resulted from the interference between two data acquisition units. Adjustments were made so the interference was eliminated for the other tests. Similar to the uniaxial creep tests results shown in Fig. 4, the three stages of the creep deformation can be found in Fig. 6. Figs. 7 (a) and (b) show the variation of the minimum displacement rate (MDR) versus the load, P, and the variation of the time to failure, t_f, versus the load, respectively. Both the correlations between MDR (mm/h) and P (kg) and the correlations between t_f (h) and P can be expressed by power laws as expressed in equations (4) and (5), respectively [6]. The fact that both of the correlations can be expressed in power law indicate that the results of the SPCT are generally of high quality and consistency.

$$\mathrm{MDR} = 6.457 \times 10^{15} P^{7.79} \quad (4)$$

$$t_f = 1.995 \times 10^{17} P^{-10.24} \quad (5)$$

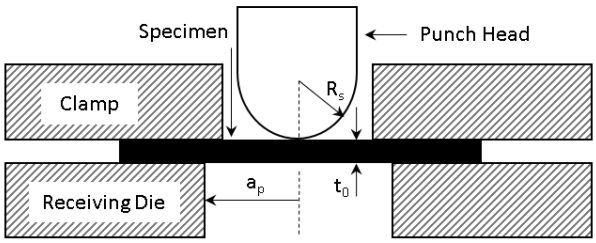

Fig. 5. Schematics of small punch test.

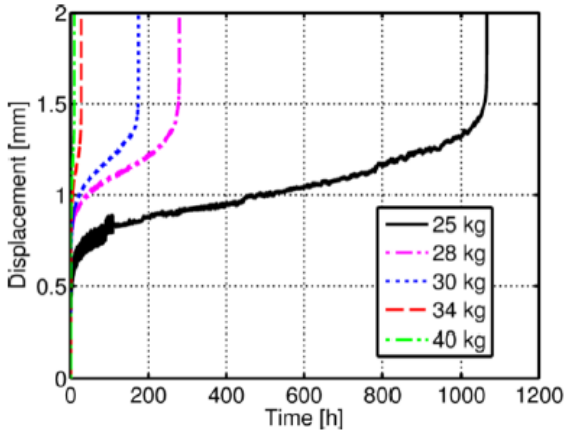

Fig. 6 Punch displacement versus time for a P91 steel at 600°C with different load levels [6].

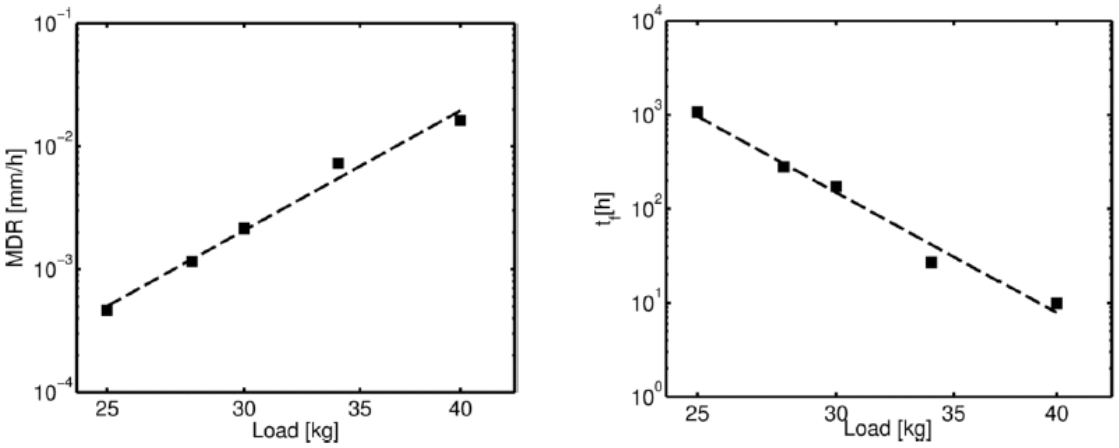

(a) (b)

Fig. 7 Logarithmic scale plots: (a) MDR versus load; (b) time to failure versus load [6].

2.2 FE Modelling

2.2.1 Material Behaviour Models

A FE model of SPCT was developed with an elastic/plastic/creep material behaviour model using the commercial code ABAQUS. The stress-strain curve from a uniaxial tensile test on a P91 steel at 600°C [29], shown in Fig. 3, was implemented in the material model in a tabular form. To simulate the creep behaviour of the material, the Liu-Murakami creep constitutive damage model [28] was employed for the FE model using a user subroutine (creep) [30]. The creep constitutive and damage evolution equations are shown as follows [28]:

$$\frac{d\varepsilon^c}{dt} = A{\sigma_{EQ}}^{N-1} exp\left[\frac{2(N+1)}{\pi\sqrt{1+\frac{3}{N}}}\left(\frac{\sigma_I}{\sigma_{EQ}}\right)^2 \omega^{3/2}\right] \qquad (6)$$

$$\frac{d\omega}{dt} = \frac{B[1-\exp(-q_2)]}{q_2}(\sigma_D)^{\chi}\exp(q_2\omega) \qquad (7)$$

$$\sigma_D = \alpha\sigma_I + (1-\alpha)\sigma_{EQ} \qquad (8)$$

where ε^c is the creep strain, t is the time, σ_{EQ}, σ_I, σ_D are the equivalent stress, the maximum principal stress and the rupture stress, ω is the creep damage state variable ($0 \le \omega \le 1$, there is no damage when $\omega = 0$ and the material is completely failed when $\omega = 1$) and A, B, χ, N, q_2, α are the constitutive creep properties. A set of typical material properties are shown in Table 2 [29], in which the creep constitutive parameters were adopted from the uniaxial creep tests data shown in Fig. 4, and they were taken as the reference material properties. The elastic modulus E was correlated to the local damage value, ω, i.e. E=E_0 $\times (1-\omega)$, E_0 is the original elastic modulus at the temperature of testing in the FE modelling.

Table 2 Creep damage constants for a P91 steel at 600°C [29].

A	B	N	χ	q_2	α
1.51×10^{-30}	2.12×10^{-27}	11.795	10.953	5.3	0.3

2.2.2 Model Geometry

The FE model was developed according to the same geometry and dimensions of the experiment setups as described in 3.3. The boundary conditions of the FE model are shown in Fig. 8. The punch and the clamps were modelled as rigid bodies, i.e. the deformation is neglected. The rotation and the horizontal displacement of the punch and the upper clamp were constrained. The radial and axial displacement and the rotation around the symmetry axis of the lower clamp were constrained. A clamp load P_{clamp}=500 kg was applied to the upper clamp and five levels of load (25 kg, 28 kg, 30 kg, 34 kg and 40 kg) were applied to the punch. The FE model of the specimen consists of 1186 bilinear axisymmetric 4-node elements with reduced integration (referred as CAX4R in ABAQUS code [30]). The FE mesh used for the simulations is shown in Fig. 9. Refined mesh was used in the region near the contact boundary between the punch and the specimen, where high stress and strain, large bending deformation and creep damage were expected. The contacts between the specimen, the punch and the clamps were defined as surface-to-surface contact interactions. The friction coefficients between the surfaces were difficult to quantify, while a generally realistic value was used for the punch/specimen contact (0.3) and the clamp/specimen contact (0.8). The geometrical non-linearity formulation was used to account for the expected large deformation during SPCT.

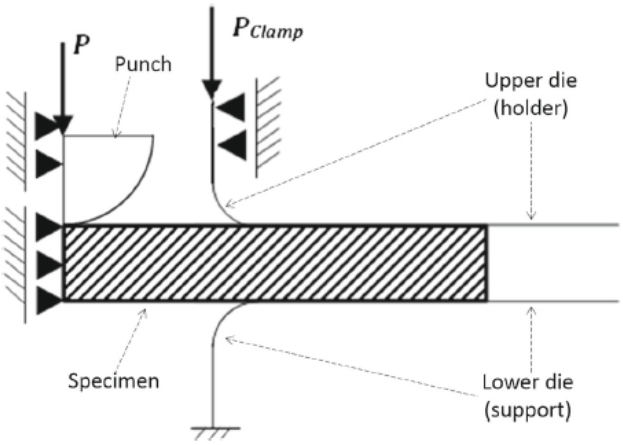

Fig. 8 Boundary conditions of the SPCT FE model.

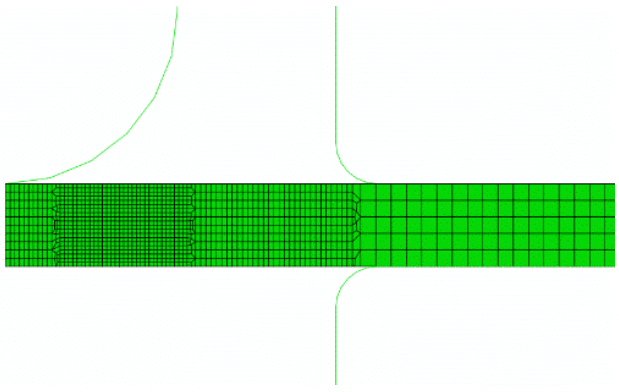

Fig. 9 FE mesh used for the SPCT simulations.

2.3 Pre-Straining Effects

The initial equivalent plastic strain (PEEQ) predicted by FE modelling at the beginning of the creep step for the load of 25kg is shown in Fig. 10. It is evident that there are nonnegligible localised plastic strains in the material, especially near the boundary of the contact region where there is a region through the thickness with the pre-strain of about 16-22% (highlighted in red colour).

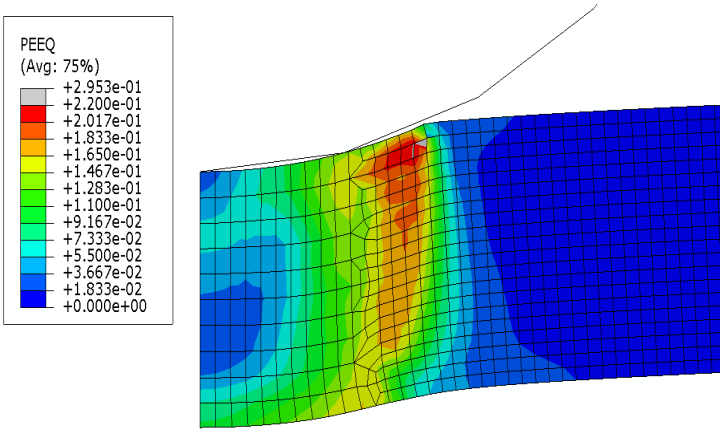

Fig. 10 Initial equivalent plastic strain contour: 25kg.

The effect of pre-straining on the creep response of various materials have been investigated by other authors [31-35]. Pre-straining effect is not negligible in many real service conditions, especially for high temperature applications for which creep or creep-fatigue is significant and dependent on the prior deformation conditions, e.g. the curved pipeline in power plants, in which high plastic strain and residual stress are induced due to manufacturing, the forged or welded aerospace components experiencing cyclic thermal and mechanical loading and combustors subject to plastic deformation and creep at low and high temperatures, respectively [31]. Some experimental studies have been designed and carried out to investigate the pre-straining effect on the creep response of some high temperature materials [31, 35]. For example, creep resistance of engineering steels and nonferrous alloys has been reported to be reduced by pre-straining [31]. It has been revealed that the creep ductility, the minimum creep strain rate and the creep failure time can all be significantly affected by pre-straining [32, 33]. In order to take pre-straining effect into consideration, a modified Liu-Murakami's creep damage model has been proposed by Cortellino et al [6]. Two parameters, ϕ and ψ, are introduced to the creep constitutive equations (equations (6) and (7)). Equations (9) and (10) show the definitions of ϕ and ψ, which account for the pre-straining effect on the minimum creep strain rate and the failure time, respectively. $\dot{\varepsilon}^{c}_{min,\ 0}$ and $t_{f,0}$ are the minimum strain rate and the failure time of material as received with no pre-straining, while the pre-strained material is referred by $\dot{\varepsilon}^{c}_{min,\ p}$ and $t_{f,p}$. When ϕ is greater than 1, the minimum strain rate of the pre-strained material increases compared to the material with no pre-strain, displaying a creep enhancement effect. On the contrary, when ϕ is less than 1, the minimum strain rate decreases when the material is pre-strained and it shows a creep resistance effect. Similarly, when ψ is greater than 1, the failure life is reduced by the pre-strain and it exhibits a creep enhancement effect, while it shows a creep resistance effect when ψ is less than 1. The modified Liu-Murakami's model is expressed as equations (11) and (12) [6].

$$\phi = \frac{\dot{\varepsilon}^{c}_{min,\ p}}{\dot{\varepsilon}^{c}_{min,\ 0}} \qquad (9)$$

$$\psi = \frac{t_{f,0}}{t_{f,p}} \qquad (10)$$

$$\frac{d\varepsilon^{c}}{dt} = \phi A {\sigma_{EQ}}^{N-1} exp\left[\frac{2(N+1)}{\pi\sqrt{1+\frac{3}{N}}}\left(\frac{\sigma_I}{\sigma_{EQ}}\right)^{2}\omega^{3/2}\right] \qquad (11)$$

$$\frac{d\omega}{dt} = \psi\frac{B[1-\exp(-q_2)]}{q_2}(\sigma_D)^{\chi}\exp(q_2\omega) \qquad (12)$$

The values of ϕ and ψ for a material can be obtained by carrying out uniaxial creep tests with different initial plastic strain. The variation of the parameters ϕ and ψ with the plastic engineering pre-strain (ε_p) are fitted to the polynomial equations (13) and (14), respectively, at various stress levels. It is easy to find that ϕ and ψ are equal to 1 when there is no pre-strain, i.e. $\varepsilon_p = 0$. The fitting coefficients were obtained from the uniaxial creep test data for different stress levels and varying amount of pre-straining [6] and then averaged to give a set of representative fitting coefficients for the material. Tables 3 and 4 show the averaged fitting coefficients for and Ψ obtained from the uniaxial creep tests on the P91 steel with different pre-strain percentages [6].

$$\phi = \exp[a_1\varepsilon_p] + b_1\varepsilon_p^2 + c_1\varepsilon_p^3 + d_1\varepsilon_p^4 \qquad (13)$$

$$\psi = \exp[a_2\varepsilon_p] + b_2\varepsilon_p^2 + c_2\varepsilon_p^3 \qquad (14)$$

Table 3 Averaged fitting coefficients for ϕ [6]

a_1	b_1	c_1	d_1
-5.9534	6.69×10^{-2}	-8.8×10^{-3}	3.236×10^{-4}

Table 4 Averaged fitting coefficients for ψ [6]

a_2	b_2	c_2
-3.241	2.61×10^{-2}	4.763×10^{-4}

The contour plots of the ϕ and ψ parameters from the FE modelling for the punch load of 25kg with the modified creep model are shown by Figs. 11 (a) and (b), respectively. The values of ϕ and ψ were calculated from equations (13) and (14) using the equivalent plastic strain at the beginning of the creep step shown in Fig. 10. It can be found that the distribution and the variation of ϕ and ψ are consistent with the equivalent plastic strain. In the region where there is zero plastic strain (the unsupported region) ϕ and ψ are equal to 1, which means there is no pre-straining effect. However, in the contact area, ϕ and ψ are less than 1, which indicates there are creep resistance effects due to pre-straining. Global creep resistance effects are revealed by the punch displacement versus time curves in Fig. 12. It shows the comparisons between the experiment

results and the results from the FEA of the SPCT on the P91 steel for the load of (a) 25kg and (b) 30kg at 600°C with and without pre-strain. For the load of 25kg, the MDR decreased about 50% and the time to failure increased about 200% when the pre-straining was included by the FE modelling, leading to a much more accurate prediction in the MDR and time to failure compared to the FE modelling without pre-strain, as Fig. 12(a) shows. Similarly, the FEA predictions of MDR and the failure time under the punch load of 30kg were both improved with the inclusion of the pre-straining effect in the FE model as shown in Fig. 12(b).

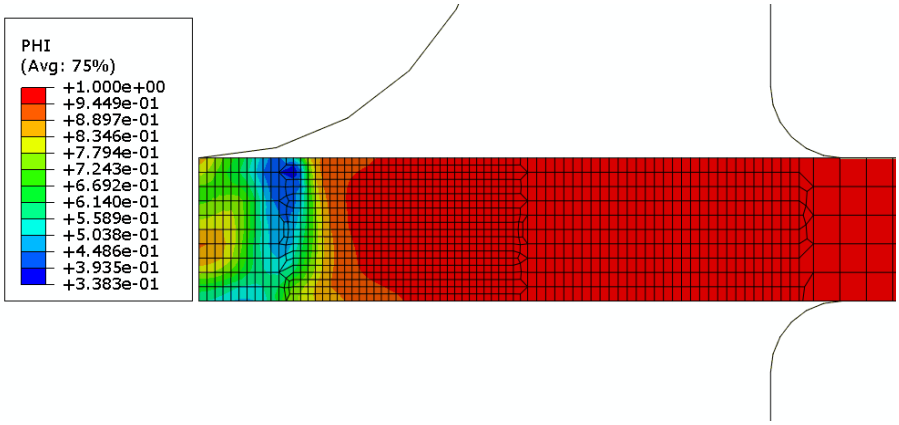

(a)

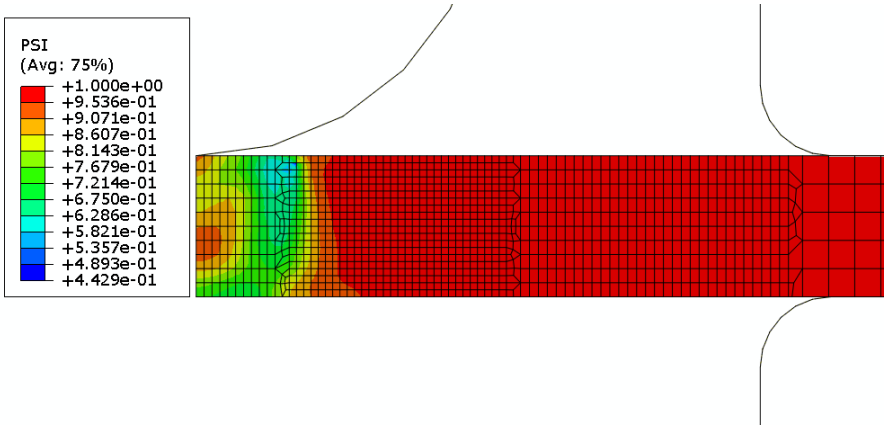

(b)

Fig. 11 FEA contours for punch load of 25kg: (a) ϕ; (b) ψ.

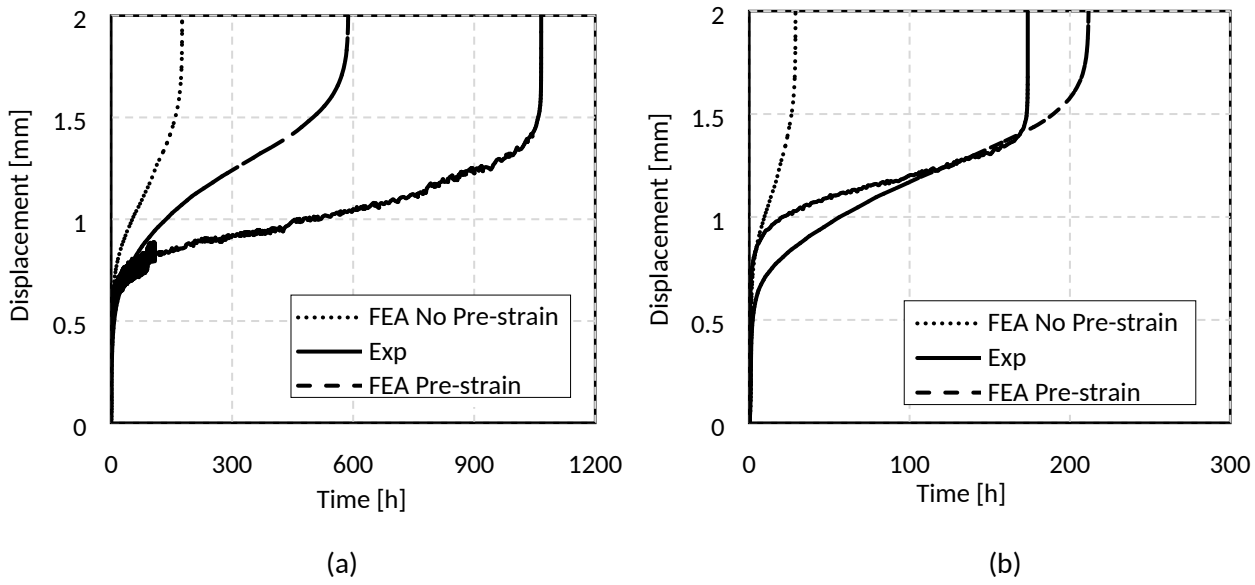

Fig. 12 Punch displacement versus time: (a) 25kg; (b) 30kg.

3. Inverse Method

3.1 Inverse Method Procedures

An inverse method was developed to determine the creep properties from the SPCT data iteratively. As it is shown in the flowchart (Fig. 13), an initial estimation of the creep properties, e.g. based on the uniaxial creep tests, was passed into the FE model to simulate SPCT at different load levels. The FE model described in sections 2.2-2.3 was applied in this study. The pre-straining effect discussed in section 2.3 was included in the inverse method for the first time. The displacement-time data is extracted from the FE results and compared to the experimental data obtained from the experiment with the corresponding load levels. The difference between the predicted and the experimental creep data (the output of the objective function, $F(x)$) is calculated and supplied as the feedback to a nonlinear least-square optimisation. The variables subjected to optimisation, i.e. the creep properties X_i, are in different orders of magnitude. Therefore, it is necessary to scale all variables to the same order of magnitude to ensure effective progress for the optimisation evolutions. Similarly, the objective quantities, i.e. errors in creep time and displacement, also need to be scaled to the same order of magnitude.

The optimisation is also subjected to nonlinear constraints shown by the constraint functions $G_1(x)$ and $G_2(x)$, i.e. MDR and time to failure, so that the MDR and time to failure obtained from FE modelling are within the predefined tolerance (tol_1, tol_2) compared to the experimental data. It should be noted that a relatively large value of tolerance might be needed to allow the initiation of the optimisation, which means a multi-step optimisation procedure might be necessary. This cycle will be continued until the variation of the objective function is within the predefined tolerance. And the inputs of the last iteration will be accepted as the optimised parameters (creep material properties).

It should be noted that the creep material properties are in very different orders of magnitude while these differences are not taken into account by the optimisation algorithm by default. Therefore, it is necessary to

scale the material properties to the same or similar orders of magnitudes. Also, the minimum step size and the magnitude of the parameter values should be in a reasonable ratio. If the step size is too small compared to the parameter values, the optimisation process may not effectively progress. On the other hand, if the changes made to the material properties are too large, then it might be difficult for the optimisation algorithm to converge to the minimum. Similarly, the objective quantities (time and displacement in this case) might also need to be scaled to the same order to ensure a relatively even contribution to the total objective function value. In addition, because the displacement rate is approximately constant in the secondary stage, while it increases rapidly in the tertiary stage of SPCT, data points were taken in a higher frequency in the tertiary stage in order to better capture the shape of the curve which will result in a better quality of convergence. The values of the parameters N and χ should be constrained within reasonable boundaries since the strain and the damage evolution are highly sensitive to these two exponents, i.e. an extreme value could lead to convergence difficulty in FE modelling for ABAQUS and the inverse analysis could be interrupted.

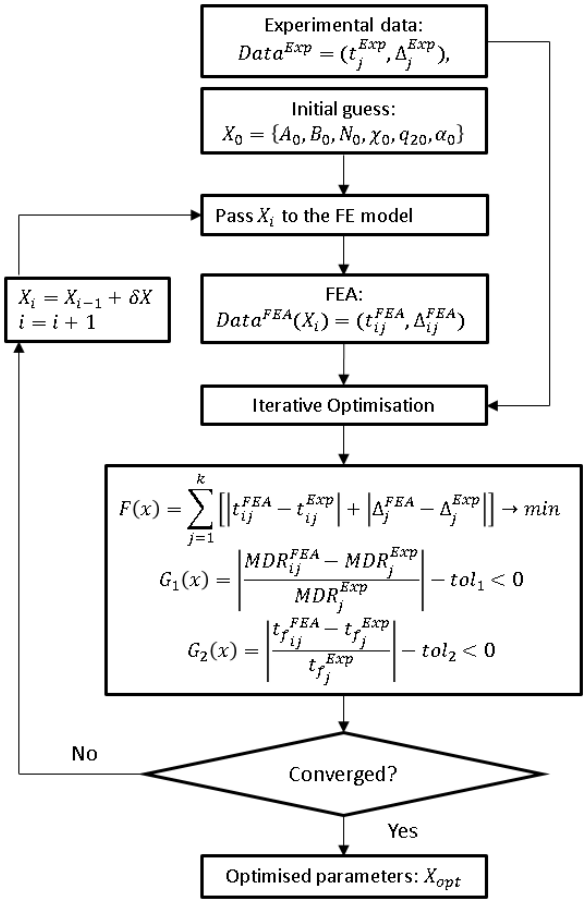

Fig. 13 Flowchart of the inverse procedures.

3.2 Application of the Inverse Method

The inverse method was applied to determine the creep properties of a P91 steel from the SPCT carried out at 600°C. The displacement-time data from the SPCT carried out at load levels of 28kg, 30kg and 34kg, shown in Fig. 6, were taken as the target curves for the optimisation process. The reference material properties presented in Table 2 were supplied to the optimisation algorithm as the initial values of the creep properties. The minimum step of the optimisation, i.e. the minimum change in the variables between two contiguous iterations, was set to be 1×10^{-5} while the variables were scaled to be in the order of 1×10^{-3}. This minimum step was selected to reduce the total computing time and it was verified that smaller step has limited effects on the FE modelling results. Because the magnitude of displacement (in unit of mm) and time (in unit of hour) were in different orders, i.e. displacement was in order of 10^{-1}-10^{0} while time was in order of 10^{1}-10^{3}, they were scaled to a similar order (10^{0}) so that the objective function value reflects the differences in displacement and time equally, instead of being dominated by the variable with the much larger magnitude (time in this case).

Fig. 14 shows the evolutions of the objective function value of the nonlinear optimisation, which is minimised from over 10000 to below 40, meaning that the optimisation has effectively converged. The optimised creep properties are shown in Table 5. The comparison between the displacement-time curves obtained from the experiments, the initial FE modelling and the final optimised FE modelling is shown in Fig. 15. The comparison between the logarithmic scale plots of the MDR and time to failure obtained from FE modelling and experiments are shown in Fig 16 (a) and (b), respectively.

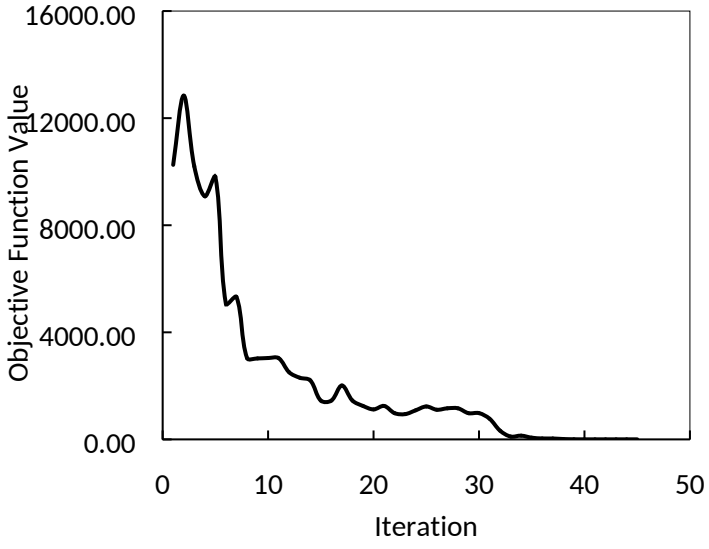

Fig. 14 Evolution of the objective function value of the nonlinear optimisation.

Table 5 Optimised creep properties for the P91 steel at 600°C

A	B	N	χ	q_2	α
2.00×10^{-31}	1.49×10^{-26}	12.11	10.85	4.85	0.215

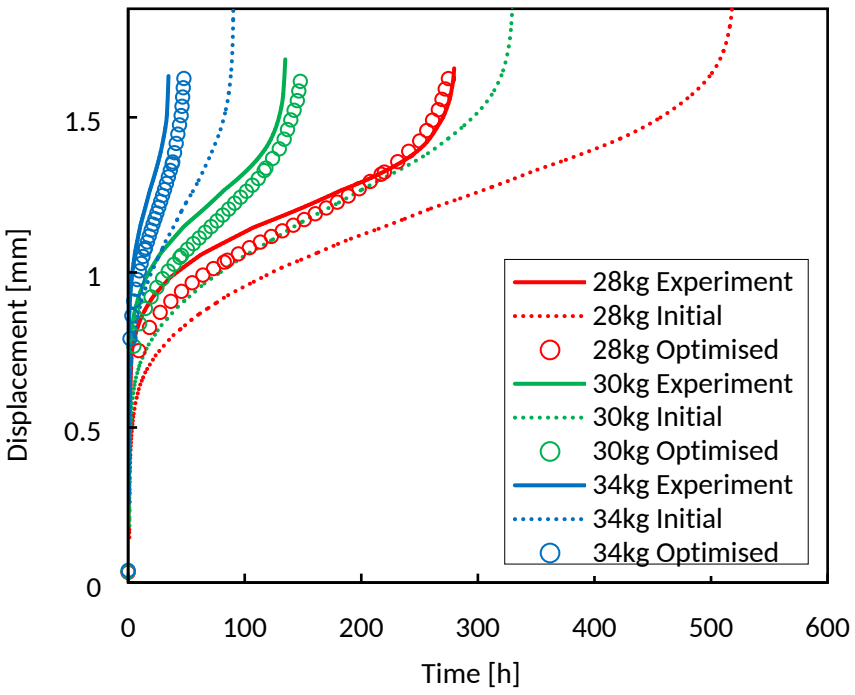

Fig. 15 Displacement-time curves from the experiments and the inverse method.

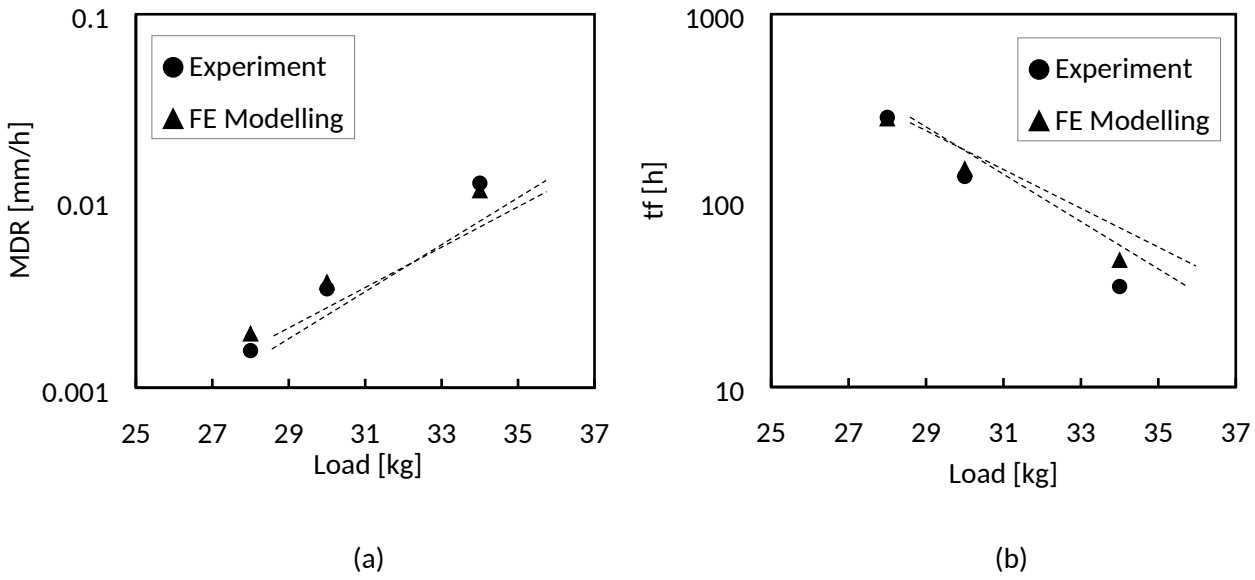

Fig. 16 Comparison between the logarithmic scale plots: (a) MDR versus load; (b) time to failure versus load.

4. Discussion

As shown by Fig. 15, it is evident that the optimised predictions of the displacement-time curves are much closer to the experimental results compared to the initial predictions at all three load levels, regarding the time to failure especially. The error percentage in time to failure for load level of 28kg is about 70% for the initial prediction while it is optimised to be within 2%. Similarly, at the load of 30kg the initial error percentage in time to failure is about 90% while it is less than 10% for the optimised prediction. However, the predicted

MDR are relatively less accurate compared to the experimental results. It should also be noted that the accuracy of the optimisation is dependent on the consistency of the experimental results at different loading levels while there is small scattering in the SPCT experiments as shown in Fig. 7. The logarithmic scale plots of the MDR and time to failure are in relatively good agreement with the experimental results, shown in Fig. 16, giving some degree of correlation for the optimised material properties.

It should be noted that the inverse method cannot guarantee to provide the unique exact solution, because the optimisation is not fully constrained although the time to failure and the minimum strain rate are applied. If additional measurements could be taken from the experiments, e.g. the strain field, stress field and microstructural evolution, which could produce solution more representative physical nature. The additional information could also help correlate the material properties determined from the experimental data. This issue has been addressed by other researchers in similar studies involving inverse method [36-38], e.g. the piling-up profile of the indented specimen, in addition to the conventional load-displacement curves, could help determine the material properties from indentation test [38]. Although the current FE model is not capable of modelling the microstructural evolution, the predicted global damage maps still provide a good correlation of the determined creep damage properties. The comparison between the predicted damage contours obtained from FE modelling with the optimised creep properties and the SEM images of the cross section of the specimen obtained from the SPCT with the punch load of 25kg interrupted at different stages is shown in Fig. 17. The evolution of the creep damage predicted by FE modelling agrees well with the SEM images, e.g. the critical creep damage initializes on the bottom surface near the contact edge and then gradually spreads through the whole section area. Also, it can be found from Fig. 17(c) that the geometry of the crack predicted by FE modelling (shown as the region with the maximum damage value) is similar to the SEM observation. Fig. 17(c) also shows a necking phenomenon near the crack predicted by the FE modelling, similar to the SEM image. These agreements between the FE modelling predictions and the SEM observations provide a validation for both the FE model considering the pre-straining effect and the inverse method developed in the current investigation.

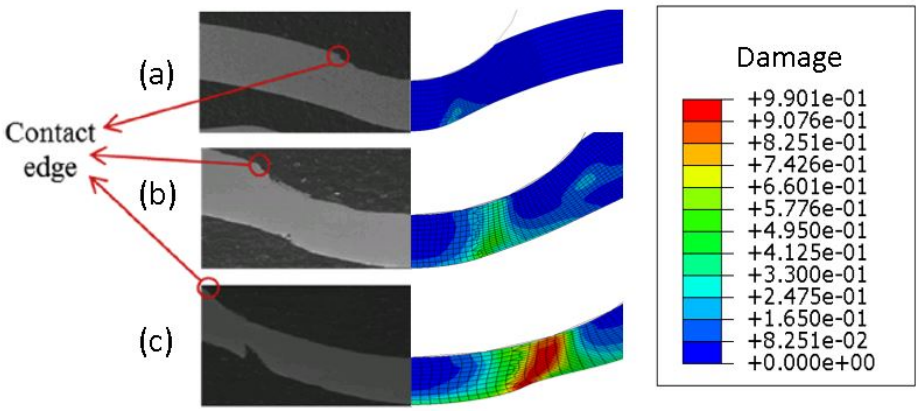

Fig. 17 SEM images from Ref. [6] for a small punch creep test on a P91 steel at 600°C with a load of 25 kg, interrupted after (a) 2h, (b) 200h and (c) 669h and the FE damage contours.

It should be noted that although the uniaxial creep properties were used as the reference properties for the application of the inverse method in this investigation, in most cases the uniaxial creep properties may not be available. In general, the initial guess for the inverse method should be estimated by using the CoP equations (1)-(3) to convert the SPCT results to uniaxial creep test results.

In the last decade, significant research on small punch creep test has been carried out with an aim to update the current CEN Code of Practice [14] which was published in 2006. One of the key aims is related to the need

for the development of improved interpretation method in order to more confidently interpret and convert the small punch data in relation to uniaxial creep properties. The method in the current CEN Code [14] was based on the Chakrabarty's membrane theory, which was unable to consider some physical features, such as continuum creep damage and the effect of initial plasticity. The present work reported in this paper is a significant step toward this objective. Due to the complex nature of the small punch creep test, physically based inverse method will form a critical part of this interpretation framework. There are a clear future need for adapting more advanced inverse optimization techniques and algorithms which may be able to include measured microstructure information, and for the development of improved constitutive models, which are capable of accurately representing the effect of visco-plasticity, and the material degradation through the use of microstructure based constitutive models, to account for the void nucleation and coalescence, micro crack formation and propagation, in order to more accurately represent the physical process of the material damage and fracture during small punch test, for the more realistic and convincing modelling.

5. Conclusions

The inverse method developed in the current investigation has been proven to be capable of extracting the material creep properties from the displacement-time data obtained from SPCT on a P91 steel at 600°C with good agreement to the experimental results. The effect of the pre-straining occurring in the early stage of SPCT has been taken into account for an inverse method for the first time. The optimised predictions in the MDR and time to failure were within an acceptable range of error percentages compared to the experimental results. Generally, the optimisation processes complete within a relatively small number of iterations meaning that the optimisation algorithm is effective and the computing time is acceptable. Also, it is for the first time to implement the elastic-plastic-Liu-Murakami damage model in the inverse analysis for SPCT.

One major concern over the inverse method with FE modelling is the cost of computing. It should be noted that it is possible to reduce the computing time for the current inverse method in the future since the FE modelling is controlled by a pre-defined step time (i.e. twice as the time to failure of the experiment at each load level) and hence there could be some unnecessary computing work as it progresses close to failure when the time increment is small and the displacement rate approaches to infinity. Also, it should be noted that the fitting coefficients for ϕ and ψ were obtained empirically from a relatively small number of tests [6], and extended experimental work in pre-strained uniaxial creep tests is expected to lead to a better estimation of ϕ and ψ parameters for the FE modelling of SPCT, hence to a further improved prediction in the creep behaviours from the inverse method developed in this investigation. A more physically representive FE model accounting for the microstructural behaviours, e.g. void nucleation, coalescence, micro crack formation and propagation, of the material during SPCT is in need for improved effectiveness of the current methodology.

Acknowledgement

This work was supported by the Engineering and Physical Sciences Research Council (EPSRC) [Grant Numbers EP/L016206, EP/M01536X/1 and EP-R000859-1]. Specific thanks go to the EPSRC Centre for Doctoral Training in Innovative Metal Processing (IMPaCT, www.impact.ac.uk).

References

[1]. Hyde TH, Sun W, Williams JA. The requirements for and the use of miniature test specimens to provide mechanical and creep properties of materials: - a review. International Material Reviews 2007; 52, 213-55.

[2]. Morris A, Cacciapuoti B, Sun W. The role of small specimen creep testing within a life assessment framework for high temperature power plant. International Material Reviews 2018; 63: 102-37.

[3]. Blagoeva D, Li YZ, Hurst RC. Qualification of P91 welds through small punch creep testing. Journal of Nuclear Materials 2011; 409: 124–30.

[4]. Gülçimen B, Hähner P. Determination of creep properties of a P91 weldment by small punch testing and a new evaluation approach. Material Science and Engineering: A 2013; 588: 125–31.

[5]. Holmstrom S, Auerkari P, Hurst R, Blagoeva D. Using small punch test data to determine creep strain and strength reduction properties for heat affected zones. Materials Science and Technology 2014; 30: 63–6.

[6]. Cortellino F, Rouse JP, Cacciapuoti B, Sun W, Hyde TH. Experimental and numerical analysis of initial plasticity in p91 steel small punch creep samples. Experimental Mechanics 2017; 57: 1193-1212.

[7]. Chen H, Hyde TH, Voisey KT, McCartney DG. Application of small punch creep testing to a thermally sprayed CoNiCrAlY bond coat, Materials Science and Engineering: A 2013; 585: 205-13.

[8]. Evans M, Wang D. The small punch creep test: some results from a numerical model. Journal of Materials Science 2008; 43: 1825–35.

[9]. Evans RW, Evans M. Numerical modelling of small disc creep test. Materials Science and Technology 2006; 22: 1155–62.

[10]. Cortellino F, Sun W, Hyde TH. On the effects of friction modelling on small punch creep test responses: a numerical investigation. Journal of Strain Analysis 2016; 51: 493-506.

[11]. Rouse JP, Cortellino F, Sun W, Hyde TH, Shingledecker J. Small punch creep testing: review on modelling and data interpretation, Materials Science and Technology 2013; 29: 1328-1345.

[12]. Hyde TH, Stoyanov M, Sun W, Hyde CJ. On the interpretation of results from small punch creep tests. Journal of Strain Analysis 2010; 45: 141–64.

[13]. Parker JD, James JD. Creep behaviour of miniature disc specimens of low alloy steel. Pressure vessels and piping conference, developments in a progressing technology 1994, Minneapolis. 279: 167-72.

[14]. CEN CWA 15627 Workshop Agreement: Small punch test method for metallic materials (Part A), European Committee for Standardization, Brussels, December 2006.

[15]. Isselin J, Iost A, Golek J, Najjar D, Bigerelle, M. Assessment of the constitutive law by inverse methodology: small punch test and hardness. Journal of Nuclear Materials 2006; 352: 97-106.

[16]. Egan P, Whelan MP, Lakestani F, Connelly MJ. Small punch test: an approach to solve the inverse problem by deformation shape and finite element optimization. Computational Materials Science 2007; 40: 33-9.

[17]. Peñuelas I, Cuesta II, Betegón C, Rodriguez C, Belzunce FJ. Inverse determination of the elastoplastic and damage parameters on small punch tests. Fatigue and Fracture of Engineering Materials and Structures 2009; 32: 872–85.

[18]. Catherine CS, Messier J, Poussard C, Rosinski S, Foulds J. Small punch test: EPRI-CEA finite element simulation benchmark and inverse method for the estimation of elastic plastic behaviour. Small Specimen Test Techniques: Fourth Volume 2002.

[19]. Yang SS, Cao Y, Ling X, Qian Y. Assessment of mechanical properties of Incoloy800H by means of small punch test and inverse analysis. Journal of Alloys and Compounds 2017; 695: 2499-505.

[20]. Soltysiak S, Selent M, Roth S, Abendroth M, Hoffmann M, Biermann H, Kuna M. High-temperature small punch test for mechanical characterization of a nickel-base super alloy. Materials Science and Engineering: A 2014; 613: 259–63.

[21]. Abendroth M. FEM analysis of small punch tests. Key Engineering Materials 2017; 734: 23-36.
[22]. Kubo Shiro, Inverse problems related to the mechanics and fracture of solids and structures. JSME International Journal, Series 1: Solid Mechanics, Strength of Materials 1988; 31: 157-166.
[23]. Schnur, DS, Zabaras, N. An inverse method for determining elastic material properties and a material interface. International Journal for Numerical Methods in Engineering 1992; 33: 2039-2057.
[24]. Kind N, Berthel B, Fouvry S, Poupon C, Jaubert O. Plasma-sprayed coatings: Identification of plastic properties using macro-indentation and an inverse Levenberg–Marquardt method. Mechanics of Materials 2016; 98: 22-35.
[25]. Wen W, Jackson GA, Li H, Sun W. An experimental and numerical study of a CoNiCrAlY coating using miniature specimen testing techniques. International Journal of Mechanical Sciences 2019; 157-158: 348-356.
[26]. Husain Asif, Sehgal DK , Pandey RK . An inverse finite element procedure for the determination of constitutive tensile behaviour of materials using miniature specimen. Computational Materials Science 2004; 31: 84–92.
[27]. Li YZ, Stevens P, Geng JF, Ma DF, Xu L. Determination of creep properties from small punch test with reverse algorithm. Key Engineering Materials 2017; 734: 212-36.
[28]. Liu Y, Murakami S. Damage localization of conventional creep damage models and proposition of a new model for creep damage analysis. JSME International Journal Series A 1998; 41: 57-65.
[29]. Saad AA, Hyde TH, Sun W, Hyde CJ, Tanner DWJ. Characterization of viscoplasticity behaviour of P91 and P92 power plant steels. International Journal of Pressure Vessels and Piping 2013; 111–112: 246–52.
[30]. ABAQUS Theory manual. Dassault SystEMes Simulia Corp 2010.
[31]. Li DF, O'Dowd NP, Davies CM, Nikbin KM. A review of the effect of prior inelastic deformation on high temperature mechanical response of engineering alloys. International Journal of Pressure Vessels and Piping 2010; 87: 531–42.
[32]. Willis M, McDonaugh-Smith A, Hales R. Prestrain effects on creep ductility of a 316 stainless steel light forging. International Journal of Pressure Vessels and Piping 1999; 76: 355–9.
[33]. Wilshire B, Willis M. Mechanisms of strain accumulation and damage development during creep of prestrained 316 stainless steels. Metallurgical and Materials Transactions A 2004; 35: 563-71.
[34]. Wilshire B, Palmer CJ. Strain accumulation during dislocation creep of prestrained copper. Materials Science and Engineering: A 2004; 387–89: 716–18.
[35]. Tai K, Endo T. Effect of pre-creep on the succeeding creep behaviour of a 2.25Cr-1Mo steel. Scripta Metallurgica et Materialia 1993; 29: 643–6.
[36]. Chen X, Ogasawara N, Zhao M, Chiba N. On the uniqueness of measuring elastoplastic properties from indentation: the indistinguishable mystical materials. Journal of the Mechanics and Physics of Solids 2007; 55: 1618–1660.
[37]. Cheng CM, Cheng YT. Can stress–strain relationships be obtained from indentation curves using conical and pyramidal indenters. Journal of Materials Research 1999; 14: 3467–3473.
[38]. Iracheta O, Bennett CJ, Sun W. A holistic inverse approach based on a multi-objective function optimisation model to recover elastic-plastic properties of materials from the depth-sensing indentation test. Journal of the Mechanics and Physics of Solids 2019; 128: 1-20.

Author Agreement

The paper is not concurrently submitted for publication elsewhere

The paper, in its entirety, in part, or in a modifies version, has not been published elsewhere

The paper has not previously been submitted for possible publication elsewhere